Automated light-based mapping of motor cortex by photoactivation of channelrhodopsin-2 transgenic mice

Oliver G S Ayling[1,2,5], Thomas C Harrison[1,2,5], Jamie D Boyd[3,5], Alexander Goroshkov[3] & Timothy H Murphy[1,2,4]

Traditionally, mapping the motor cortex requires electrodes to stimulate the brain and define motor output pathways. Although effective, electrode-based methods are labor-intensive, potentially damaging to the cortex and can have off-target effects. As an alternative method of motor mapping, we photostimulated transgenic mice expressing the light-sensitive ion channel channelrhodopsin-2 in predominantly layer-5 output cortical neurons. We report that optical stimulation of these neurons _in vivo_ using a stage scanning laser system resulted in muscle excitation within 10–20 ms, which can be recorded using implanted electromyogram electrodes or by a noninvasive motion sensor. This approach allowed us to make highly reproducible automated maps of the mouse forelimb and hindlimb motor cortex much faster than with previous methods. We anticipate that the approach will facilitate the study of changes in the location and properties of motor maps after skilled training or damage to the nervous system.

The motor cortex was the first region of the brain to be mapped and to have an overt function attributed to it[1]. Motor mapping technologies have been refined in the intervening years and now include intracortical microstimulation (ICMS)[2] and surface stimulation with electrode arrays[3]. The advent of transcranial magnetic stimulation has made noninvasive motor mapping feasible in humans[4]. Each of these techniques has unique advantages and limitations. Transcranial magnetic stimulation is noninvasive but has poor spatial resolution. Electrode-based brain stimulation methods have common disadvantages: the inability to selectively target neuronal subtypes, indiscriminate activation of axons of passage and damage when impalements are made.

Recently it has become possible to stimulate neurons using light, either by uncaging neurotransmitters[5,6] or by directly activating light-sensitive channels[7,8]. Channelrhodopsin-2 (ChR2) is a light-activated nonselective cation channel isolated from the green alga _Chlamydomonas reinhardtii_[9], which when expressed in neurons can transduce light energy into neural activity[10]. Here we present hardware and software for light-based mapping (LBM) of motor cortex output from anesthetized mice expressing ChR2 (ref .11). High-resolution motor maps are generated quickly, reliably and accurately in mice using a stage scanning system and fixed laser. We offer investigators a tool with greatly improved speed and precision to interrogate the motor cortex and address questions about sensorimotor processing both in the normal brain and after training, injury or disease.

RESULTS

Automated mapping of motor cortex using laser light

For automated ChR2-based motor mapping we chose a relatively collimated 473 nm laser targeted through a simple microscope (**Fig. 1a**). To check the beam profile as it passes through brain tissue, we directed the beam into the cortical surface of a fixed mouse brain section (**Fig. 1b**). The beam width (measured using a monochrome camera) was 170 ± 3.7 μm at the cortical surface and 640 ± 220 μm at a depth of 250 μm ($n = 7$ measurements; all values are reported as mean $\pm$ s.d.; **Fig. 1c**). Examination of light intensity at different depths indicated that beam width decreased exponentially with a decay constant of ~ 450 μm.

For LBM, we moved the mouse relative to the laser using a fast scanning stage (13 mm s^{-1})[12]. We moved the stage in random order to each of the predefined stimulation locations superimposed on the cortical map (**Fig. 1a**), and delivered a flash of laser light to each point while collecting an electromyogram (EMG) and a cortical electroencephalogram (EEG). We selected the intensity and duration of photostimulation based on their ability to elicit a suprathreshold EMG response.

Photostimulation elicited homogeneous cortical excitation

After verifying that the stage scanning laser system was accurate in positioning, we tested its ability to evoke local excitation of the cortex by performing a craniectomy and then placing surface EEG electrodes made of silver wire in the four corners of the craniectomy. We mapped EEG responses over areas of up to 20 mm^2 divided into activation sites of ~ 0.09 mm^2 (300 μm spacing) and found that photostimulation excited all regions of the exposed cortex (**Fig. 2a–c**). Homogeneity of cortical excitation ensured that
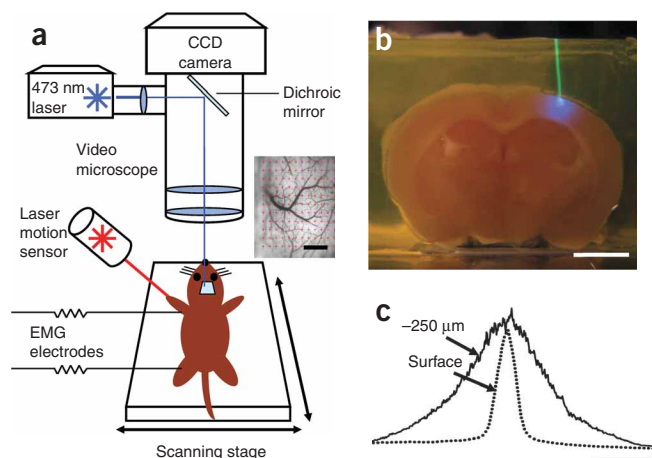
Figure 1 | Automated LBM of the mouse motor cortex. (**a**) Experimental setup. Anesthetized mice were placed on a scanning stage and an array of cortical points (inset) was stimulated by a 473 nm collimated laser beam directed through a video microscope objective. Motor output was detected by EMG electrodes in forelimb and hindlimb muscles, and by a laser motion sensor fixed to the stage. (**b**) Photograph of a stimulation laser targeted at a coronal slice of fixed brain tissue embedded in carboxyfluorescein-containing agarose. (**c**) Intensity profile of the illuminated area as the beam passes through fluorescent agarose above the surface of the brain and 250 μm under the cortical surface (peaks were normalized for comparison). Images used for analysis were acquired using a high-resolution monochromatic camera. Scale bars, 1 mm (**a**), 2 mm (**b**) and 400 μm (**c**).

differences in motor maps reflect local motor output circuitry and not the distribution of ChR2 responsiveness.

In evaluating EEG recordings, we found that photostimulation as short as 1–5 ms evoked a response. These brief light flashes produced cortical depolarizations that were significantly longer than the stimulus duration (31.4 ± 5.4 ms, $P < 0.0001$, $n = 15$ trials in four mice, unpaired t-test; **Fig. 2d**). We also found that targeting the laser at the exposed EEG electrode caused a large photoelectric artifact that was different in kinetics from the results of cortical tissue excitation and was restricted to periods when the laser was activated. As expected, wild-type mice lacking ChR2 showed no response to photostimulation ($n = 6$) but did show the photoelectric artifact (**Supplementary Fig. 1** online).

To confirm the expression of ChR2-YFP protein reported by the developers of the mouse[11] and the distributor (Jackson Labs), we performed a histological examination of ChR2-YFP fluorescence in a subset of mice ($n = 3$; **Supplementary Fig. 2** online). We corroborated the homogeneous distribution of ChR2-YFP fusion protein throughout the sensorimotor cortex and its restriction to tufted layer-5 neurons as originally reported, and this was consistent with other *Thy1* promoter–driven mouse lines[11,13]. In two mice examined by confocal microscopy we saw no labeling of neuronal cell bodies in more superficial layers (**Supplementary Fig. 2**).

Mapping light-evoked muscle potentials in ChR2 mice

By implanting silver EMG electrodes in the triceps brachii (extensor) and extensor carpi radialis brevis muscles of the forelimb, and the biceps femoris (flexor) and vastus lateralis (extensor) of the hindlimb, we established the parameters of LBM necessary to evoke contralateral EMG responses. We assessed the effect of light intensity (40–600 mW mm^{-2}) and stimulus duration (1–35 ms), and found that these ranges of intensity and duration were sufficient to produce a motor response (**Fig. 2d**). Photoactivation of areas 170 μm in diameter reliably evoked a motor cortex EEG response and a delayed EMG response in contralateral forelimb and contralateral hindlimb muscles. We did not study smaller photoactivation areas because the arbors of layer-5 neurons are at least 300 μm across, and we would not expect any increase in detail with reduced photoactivation areas.

We assigned processed EMG responses a grayscale value on a linear scale from black (zero) to white (maximum response) to form a pixel-based map, typically created with grids of stimulation

points using 300 μm spacing (**Fig. 3a–d** and **Supplementary Methods** online). Given some scattering of blue light by tissue[14], this spatial frequency should efficiently excite the cortex between each of the points and is consistent with photoactivation areas used in previous brain-slice and *in vivo* work[11,14].

Photostimulation in the center of motor maps yielded muscle excitation after a delay from the photostimulation onset of 10.8 ± 1.0 ms for contralateral forelimb and 19.4 ± 1.0 ms for contralateral hindlimb EMG ($n = 4$ mice). Analysis of the relationship between cortical EEG depolarization and evoked EMG signals (**Fig. 2d**) revealed the latency between cortical excitation and muscle excitation. As expected, optically evoked EMG responses exhibited latencies comparable to those of EMG responses produced by direct electrode-based stimulation of motor cortex in mice and other animals (**Fig. 3e,f**)[15]. In ICMS experiments, the latency of ICMS-evoked EMG responses was 11.1 ± 1.1 ms for contralateral forelimb and 19.5 ± 0.9 ms for contralateral hindlimb ($n = 4$ mice), consistent with values from photostimulation experiments. Cortical regions from which LBM evoked larger EMG responses tended to also produce responses with shorter latencies (**Supplementary**
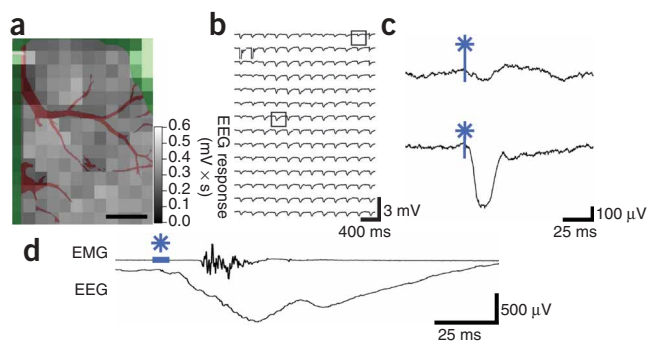

Figure 2 | ChR2-mediated EEG responses can be elicited from all regions of the exposed cortex. (**a**) Mean EEG responses evoked when the laser stimulated that cortical location from four electrodes at the cortical surface. EEG amplitudes were normalized to the maximum value (within each electrode), and then the mean values from all four electrodes were averaged. Lighter colors signify a larger response. The linear scale was set to emphasize variations in cortical response. At points of stimulation where the cortical surface was obstructed by blood vessels or bone (colored red and green, respectively), responses were diminished or absent. Scale bar, 1 mm. (**b**) Raw EEG traces from a single electrode. (**c**) Traces (boxed in **b**) showing a representative EEG response evoked by stimulation over bone (top) and of exposed cortex (bottom). Optical stimulation began at the point marked by the asterisk. (**d**) The relative time courses of ChR2-evoked EEG and EMG responses are shown after a single 5 ms pulse of 160 mW mm^{-2} laser light (blue bar). Note the prolonged EEG depolarization relative to stimulus duration.
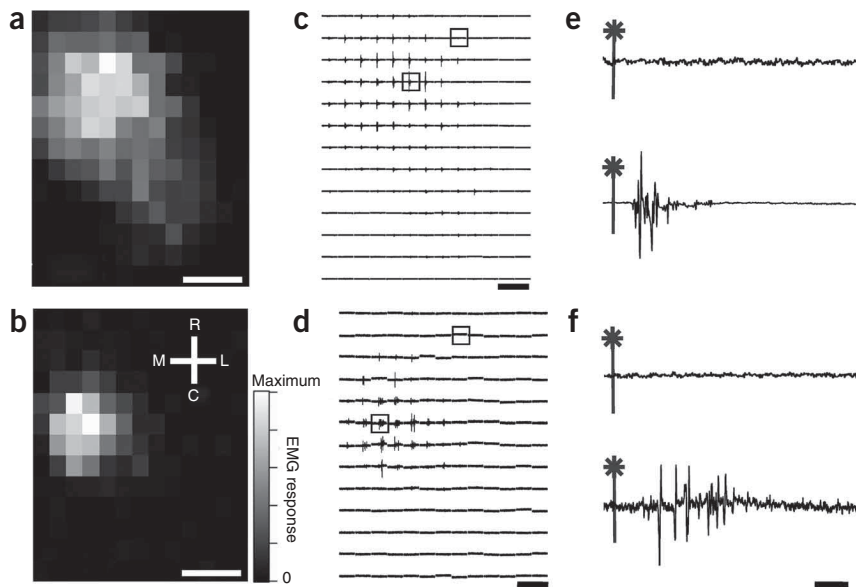
Figure 3 | High-resolution optically stimulated motor maps. (**a,b**) Forelimb triceps brachii (**a**) and hindlimb biceps femoris (**b**) motor maps created with 320 µm spacing between laser stimulation points (single 15 ms pulses at 160 mW mm^{-2}). Each map is the average of three repetitions. Absolute grayscale values are not equivalent for **a** and **b**. M, medial; L, lateral; R, rostral; and C, caudal. (**c,d**) One repetition of raw EMG traces for forelimb (**c**) and hindlimb (**d**), with individual traces arranged according to the cortical locations from which they were evoked by photostimulation. (**e,f**) Boxes in **c** and **d** identify expanded forelimb (**e**) and hindlimb (**f**) EMG traces with an asterisk indicating the onset of laser stimulation. Responses to optical stimulation of points outside the motor maps (top traces) and inside the motor maps (bottom traces) are shown. Scale bars, 1 mm (**a,b**), 200 ms (**c,d**) and 20 ms (**e,f**).

Fig. 3 online). In a mouse on which we performed both ICMS and LBM (**Fig. 4**), the positions and sizes of motor maps were generally in agreement. In this combined ICMS and LBM experiment we performed 26 penetrations to map the motor cortex, completing the ICMS map in approximately 1 h. In the same amount of time, we could map more than 3,000 points using LBM.

Given that layer-5 neurons make corticospinal projections, it is likely that LBM does not require intracortical excitatory synaptic activity to stimulate muscles. Application of α-amino-3-hydroxyl-5-methyl-4-isoxazole-propionate (AMPA) and N-methyl-D-aspartic acid (NMDA)-type glutamate receptor antagonists (**Supplementary Methods** and **Supplementary Fig. 4** online) directly to the sensorimotor cortex at concentrations and durations previously shown to block sensory signals[16] suggested that LBM activates corticofugal projections directly and not antagonist-sensitive circuitous intracortical routes of motor activation.

To estimate the area of cortex activated by light pulses, we examined intrinsic optical signals (IOS) in response to 100 ms trains of light pulses and found them to spread over $1,012 \pm 316$ µm ($n = 4$ mice, measured at full width at half-maximal amplitude; **Supplementary Methods** and **Supplementary Fig. 5** online) consistent with the extent of light scattering observed at a depth of 250 µm (**Fig. 1c**). In comparison, we observed ICMS electrode activation widths of 690 ± 102 µm ($n = 3$ mice), indicating that LBM activates an area only moderately larger than ICMS (~ 2.2-fold larger). The IOS response area within a contour plot drawn at 75% of the peak laser activation was considerably smaller (0.22 mm^2 or about 0.5 mm in diameter; **Supplementary Fig. 5**). These measurements suggest relative differences between ICMS and LBM activation areas; however, the use of IOS activation area to determine exactly what fraction of output neurons are activated with a single light pulse may be complicated by potential non-linearity associated with IOS measurements and by uncertainty of the relevant firing thresholds.

Regarding phototoxicity, we observed no consistent decrease in the amplitudes of evoked EEGs or EMGs during an experiment and no gross histological evidence of damage. In two mice involved in particularly long experiments, EMG amplitude showed no
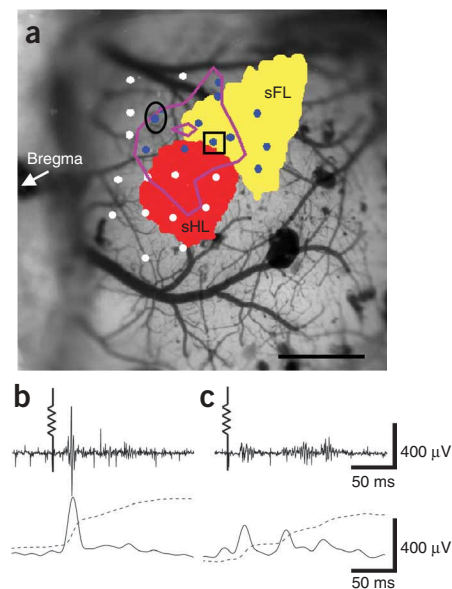
measurable reduction after >100 stimulus repetitions made over the same areas (**Supplementary Fig. 6** online). By making a sealed chronic cranial window and using a noninvasive laser–based measurement device[17] we found in two preliminary experiments that similar forelimb movement maps could be evoked in sessions 7–10 d apart, indicating that LBM does not lead to slowly developing toxicity (**Supplementary Fig. 7** online). The laser motion sensor was more sensitive to paw movements than visual assessment and provided data on an absolute scale that agreed with EMG-based maps (**Supplementary Fig. 8** online).

Figure 4 | ICMS and LBM motor maps obtained from the same ChR2-positive mouse. (**a**) Points of electrode-based ICMS trains are displayed in blue (forelimb movement) and white (no forelimb movement). Purple contour lines represent the ChR2-derived LBM forelimb motor map created with single 20 ms, 160 mW mm^{-2} laser pulses (90% and 50% of peak response). IOS sensory maps are displayed in yellow for sensory forelimb sFL and red for sensory hindlimb sHL. Scale bar, 1 mm. (**b,c**) Raw EMG (top), full wave rectified response (bottom, solid line) and integrated response (bottom, dashed line) for the ICMS point of stimulation marked in **a** by the square (**b**) and the oval (**c**). Electrode symbol indicates stimulus onset.
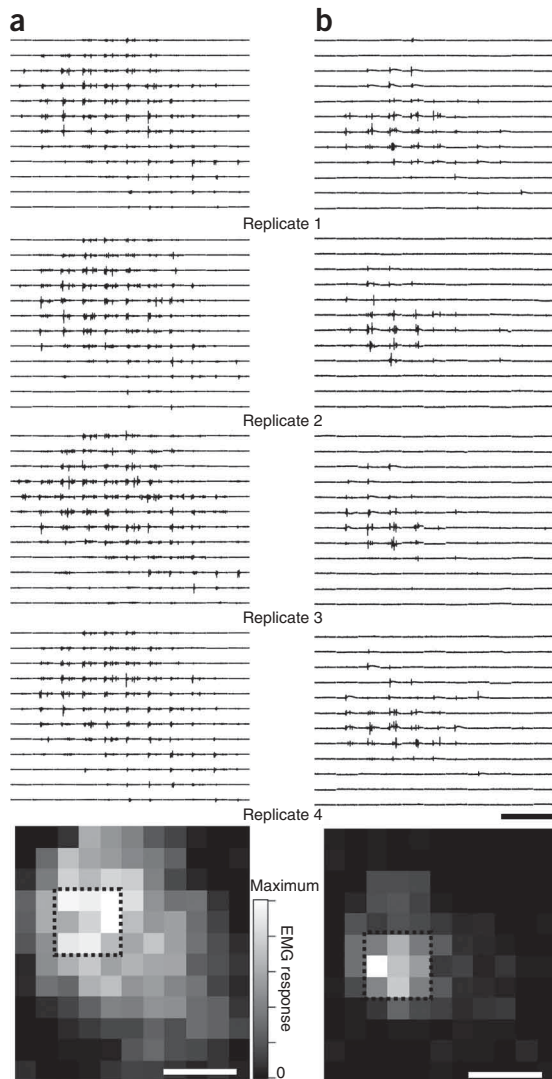
Figure 5 | Motor maps are stable and repeatable. (**a**,**b**) Four consecutive replicates (numbered) of forelimb (**a**) and hindlimb (**b**) EMGs in response to laser stimulation using 10 ms, 160 mW mm^{-2} blue-light pulses. The resulting four motor maps were generated in ~100 s per repetition. In each array, individual EMG traces (200 ms long) are plotted according to the stimulation position from which they were evoked. These spatial relationships are preserved in the pixel-based maps of response amplitude. The mean response within a 9-pixel region of interest at the center of each map (as defined by two-dimensional Gaussian fit) was 38.4 ± 10.0 mV × ms for contralateral hindlimb and 848 ± 74.3 mV × ms for contralateral forelimb. Stimulation was performed with 300 μm spacing between points, and each pixel represents a cortical area of 0.09 mm^2. Scale bars, 500 ms (top) and 1 mm (bottom).

separated from the center of the combined hindlimb map by an average distance of 0.46 ± 0.25 mm ($P = 0.0005$, $n = 9$ mice, one-sample two-tailed t-test). Our map analysis suggests that muscles working together to control a body part were represented in very similar regions of motor cortex, whereas muscles in different appendages overlapped less. In eight mice we defined map coordinates with reference to bregma (**Supplementary Table 1** online).

We examined the spatial relationships between sensory and motor representations of contralateral forelimb and contralateral hindlimb ($n = 3$ mice; **Fig. 6**). Approximately 50% of contralateral forelimb and contralateral hindlimb motor maps overlapped with sensory cortex (**Supplementary Table 2** online). Although there is some uncertainty about the motor map edge position (to within 500 μm), the motor and sensory map center positions should be more precise. The distances between the centers of the forelimb motor and sensory maps were 1,217 ± 669 μm, and centers of hindlimb motor and sensory maps were 540 ± 454 μm apart.

DISCUSSION

Given that electrode impalements require several minutes each, we estimate that LBM is two orders of magnitude faster than electrode-based techniques. We anticipate that such an approach will be useful for determining changes in motor map structure before and after stroke or spinal cord injury[18–20].

Although we performed mostly acute experiments, LBM is ideally suited to longitudinal experiments and can be performed multiple times on the same mouse through a chronic craniectomy[21]
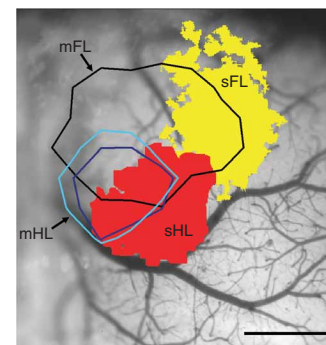
Fine motor map structure

Repeated LBM maps from the same mouse indicated that spatial heterogeneity in EMG amplitude was not due to noise or poor sampling but reflected the underlying properties of the motor representations (**Fig. 5**). To examine limb representations on a finer scale, we compared the size and center positions of two different muscles within a motor map of a single limb by one-way ANOVA ($P = 0.0007$) and Tukey post-hoc tests. Contralateral forelimb extensor muscle maps were similar in size when thresholded at 50% of maximal amplitude (**Supplementary Methods**): carpi radialis brevis and triceps brachii muscle maps were 1.65 ± 0.61 mm^2 ($n = 9$ mice) and 1.60 ± 0.67 mm^2 ($n = 7$), respectively ($P >$ 0.05). The same was true for the hindlimb biceps femoris flexor and vastus lateralis extensor maps (0.71 ± 0.30 mm^2 ($n = 5$) and 0.61 ± 0.28 mm^2 ($n = 7$), respectively; $P >$ 0.05). Both contralateral forelimb maps were significantly larger than either of the contralateral hindlimb maps ($P <$ 0.05), which is consistent with epidural array-based mapping studies in the rat[3]. Similar to map area, differences in motor map position were significant only when comparisons were made between contralateral forelimb and contralateral hindlimb, and not between muscles within the same limb. Forelimb muscle representations had a mean center point that was

Figure 6 | Motor and sensory cortical limb representations. Sensory forelimb (sFL) and sensory hindlimb (sHL) representations were visualized using IOS imaging (thresholded at 50% of maximal response). Contour lines at 50% of peak response are shown for the extensor carpi radialis forelimb muscle (mFL) and the hindlimb biceps femoris (mHL) and vastus lateralis (dark blue) motor maps derived from single 5 ms, 330 mW mm^{-2} laser pulses. Scale bar, 1 mm.

or possibly a thinned-skull preparation[22]. Notably, we observed some activation through thinned bone at the edge of the craniectomy (**Supplementary Fig. 7**). Repeated ICMS (on the same rat) has been conducted in the past[23,24], but the likelihood of damaging the brain makes LBM a better choice for longitudinal studies of reorganization following experimental manipulations.

Other advantages of LBM over penetrating electrodes are related to sampling. With LBM, stimulation points can be arrayed in a perfect grid, ensuring a more uniform sampling of the cortex than is possible with ICMS. We found that the presence of large blood vessels did not completely block the photoactivation of ChR2, and that motor maps could be obtained even in areas occupied by large vessels, something that would not be possible with ICMS (**Fig. 2a**).

LBM appears to detect motor representations selectively as the resulting forelimb and hindlimb motor maps were located medial to the respective sensory maps (**Fig. 6**) in the approximate location expected for the mouse motor cortex[17,25] and in agreement with observations in rats[3]. Although the size and center of the forelimb and hindlimb motor representations were different, the two territories exhibited considerable spatial overlap. Possibly motor map overlap between limbs could reflect activation at off-target sites resulting from light scattering or spatial overlap between axonal or dendritic arbors of forelimb and hindlimb motor cortex. Alternatively, map overlap may be physiologically relevant and would suggest that specificity in motor output is achieved through additional regulation and not just the topographical layout of the motor cortex. Conceivably, LBM could be extended to single neurons to address whether excitation of individual neurons[26] within overlapping map areas can evoke both forelimb and hindlimb muscle excitation, or whether individual neurons are dedicated to specific limbs. Notably, we have shown previously that reorganization after a stroke can cause individual somatosensory neurons (normally preferentially activated by signals from a single limb) to process information from multiple limbs, suggesting that single neurons can assume multiple roles[20]. With regard to sensory maps, LBM shows that the centers of sensory and motor maps are generally ~0.5–1 mm apart (**Fig. 6**), supporting lower-resolution studies using ICMS in rats that had identified these areas as a mixed sensorimotor cortex[27,28].

The resolution of LBM depends on its ability to activate subsets of cortex despite the scattering of light and despite the presence of overlapping axons and dendrites from neurons with cells bodies outside of the activation area. Estimation of the cortical area LBM activates is a complex function of light scattering and depth-dependent changes in excitability. However, we can define a lower limit based on the size of the hindlimb motor map we observed (~0.65 mm^2 or 0.9 mm in diameter). We estimated the area of cortex activated by LBM pulses using IOS imaging. The area showing > 50% of maximal activation was approximately 0.8 mm^2 (measured at full width at half-maximal amplitude), about the size of the hindlimb motor map. Notably, IOS activation profiles of point-source ICMS electrodes were also relatively large, indicating that improvements in light delivery may not lead to large gains in resolution. Given that excitation of motor neurons would not be linearly related to IOS changes and that the method does not directly read out activity within output neurons, it is possible that the spatial resolution of LBM is substantially greater than we

estimated. Despite some uncertainty about map edge position, map center positions would be expected to be more precise and should accurately define the location of motor maps and potential changes after experimental manipulations. To improve the resolution of LBM, future work could use red-shifted variants of ChR2 (ref. 29) using wavelengths of light that are less susceptible to scattering in tissue. Perhaps the largest gain in resolution would be from making a transgenic rat with ChR2 expression driven by the *Thy1* promoter, where the motor cortex would be at least threefold larger[23].

Most previous motor-mapping studies have been conducted in rats or other larger species, but the variety of available transgenic mice makes them an increasingly attractive experimental model. As other strains become available, it will be interesting to conduct motor or intracortical mapping studies using mice that express ChR2 in other cortical layers or groups of neurons. LBM could also be extended to more complex movements using patterned stimulation or multisite activation[30].

METHODS

Mouse preparation, anesthesia and optical stimulation parameters. Animal protocols were approved by the University of British Columbia Animal Care Committee. Channelrhodopsin-2 transgenic mice[11] were purchased from the Jackson Labs (line 18, stock 007612, strain B6.Cg-Tg(Thy1-COP4/EYFP)18Gfng/J). After craniectomy, the mouse was fixed to the scanning stage, and the locations of its somatosensory forelimb and hindlimb representations were visualized using IOS imaging[20]. During craniectomy surgery and IOS imaging the mouse was anesthetized with isoflurane (1.5% in air). Ketamine-xylazine (100 mg kg^{-1} ketamine, 10 mg kg^{-1} xylazine) anesthetic was used during motor mapping. We generally collected several cortical EEG-based maps at the beginning of each experiment using low laser power (40 mW mm^{-2}) and short activation duration (1 ms). In some cases when responses were weak (usually when craniectomies were imperfect), we increased laser power (up to 200 mW mm^{-2}) and/or duration (up to 5 ms). We then connected the EMG electrodes and laser motion sensor, and began collecting motor maps. These EMG experiments were typically conducted using increased laser power (40–600 mW mm^{-2}) and duration (up to 35 ms), with stimulus parameters adjusted to suprathreshold levels.

Additional methods. Descriptions of surgeries, photostimulation, imaging, ICMS, EEG and EMG recording, software and data analysis are available in **Supplementary Methods**.

Note: Supplementary information is available on the Nature Methods website.

AUTHOR CONTRIBUTIONS
O.G.S.A. and T.C.H. collected and analyzed data, and prepared the manuscript. J.D.B. developed software, analyzed data and performed histological analyses. A.G. performed optical design and fabrication of the device. T.H.M. conceived the work, analyzed data and prepared the manuscript.

COMPETING INTERESTS STATEMENT
The authors declare competing financial interests: details accompany the full-text HTML version of the paper at http://www.nature.com/naturemethods/.

1. Penfield, W. & Boldrey, E. Somatic motor and sensory representation in the cerebral cortex of man as studied by electrical stimulation. *Brain. J. Neurol.* **60**, 389–443 (1937).
2. Donoghue, J.P. & Sanes, J.N. Peripheral-nerve injury in developing rats reorganizes representation pattern in motor cortex. *Proc. Natl. Acad. Sci. USA* **84**, 1123–1126 (1987).
3. Hosp, J.A. *et al.* Thin-film epidural microelectrode arrays for somatosensory and motor cortex mapping in rat. *J. Neurosci. Methods.* **172**, 255–262 (2008).
4. Siebner, H.R. & Rothwell, J. Transcranial magnetic stimulation: new insights into representational cortical plasticity. *Exp. Brain Res.* **148**, 1–16 (2003).
5. Shepherd, G.M.G., Pologruto, T.A. & Svoboda, K. Circuit analysis of experience-dependent plasticity in the developing rat barrel cortex. *Neuron* **38**, 277–289 (2003).
6. Luo, L., Callaway, E.M. & Svoboda, K. Genetic dissection of neural circuits. *Neuron* **57**, 634–660 (2008).
7. Huber, D. *et al.* Sparse optical microstimulation in barrel cortex drives learned behaviour in freely moving mice. *Nature* **451**, 61–64 (2008).
8. Zhang, F., Aravanis, A.M., Adamantidis, A., de Lecea, L. & Deisseroth, K. Circuit-breakers: optical technologies for probing neural signals and systems. *Nat. Rev. Neurosci.* **8**, 577–581 (2007).
9. Nagel, G. *et al.* Channelrhodopsins: directly light-gated cation channels. *Biochem. Soc. Trans.* **33**, 863–866 (2005).
10. Boyden, E.S., Zhang, F., Bamberg, E., Nagel, G. & Deisseroth, K. Millisecond-timescale, genetically targeted optical control of neural activity. *Nat. Neurosci.* **8**, 1263–1268 (2005).
11. Arenkiel, B.R. *et al.* In vivo light-induced activation of neural circuitry in transgenic mice expressing channelrhodopsin-2. *Neuron* **54**, 205–218 (2007).
12. Callaway, E.M. & Katz, L.C. Photostimulation using caged glutamate reveals functional circuitry in living brain-slices. *Proc. Natl. Acad. Sci. USA* **90**, 7661–7665 (1993).
13. Feng, G.P. *et al.* Imaging neuronal subsets in transgenic mice expressing multiple spectral variants of GFP. *Neuron* **28**, 41–51 (2000).
14. Aravanis, A.M. *et al.* An optical neural interface: in vivo control of rodent motor cortex with integrated fiberoptic and optogenetic technology. *J. Neural Eng.* **4**, S143–S156 (2007).
15. Rho, M.J., Lavoie, S. & Drew, T. Effects of red nucleus microstimulation on the locomotor pattern and timing in the intact cat: a comparison with the motor cortex. *J. Neurophysiol.* **81**, 2297–2315 (1999).
16. Murphy, T.H., Li, P., Betts, K. & Liu, R. Two-photon imaging of stroke onset in vivo reveals that NMDA-receptor independent ischemic depolarization is the major cause of rapid reversible damage to dendrites and spines. *J. Neurosci.* **28**, 1756–1772 (2008).
17. Ferezou, I. *et al.* Spatiotemporal dynamics of cortical sensorimotor integration in behaving mice. *Neuron* **56**, 907–923 (2007).
18. Raineteau, O. & Schwab, M.E. Plasticity of motor systems after incomplete spinal cord injury. *Nat. Rev. Neurosci.* **2**, 263–273 (2001).
19. Brown, C.E., Li, P., Boyd, J.D., Delaney, K.R. & Murphy, T.H. Extensive turnover of dendritic spines and vascular remodeling in cortical tissues recovering from stroke. *J. Neurosci.* **27**, 4101–4109 (2007).
20. Winship, I.R. & Murphy, T.H. In vivo calcium imaging reveals functional rewiring of single somatosensory neurons after stroke. *J. Neurosci.* **28**, 6592–6606 (2008).
21. Trachtenberg, J.T. *et al.* Long-term *in vivo* imaging of experience-dependent synaptic plasticity in adult cortex. *Nature* **420**, 788–794 (2002).
22. Xu, H.T., Pan, F., Yang, G. & Gan, W.B. Choice of cranial window type for *in vivo* imaging affects dendritic spine turnover in the cortex. *Nat. Neurosci.* **10**, 549–551 (2007).
23. Kleim, J.A. *et al.* Functional organization of adult motor cortex is dependent upon continued protein synthesis. *Neuron* **40**, 167–176 (2003).
24. Teskey, G.C., Monfils, M.H., VandenBerg, P.M. & Kleim, J.A. Motor map expansion following repeated cortical and limbic seizures is related to synaptic potentiation. *Cereb. Cortex.* **12**, 98–105 (2002).
25. Franklin, K.B.J. & Paxinos, G. The mouse brain. In *Stereotaxic Coordinates* (Academic Press, New York, 1997).
26. Herfst, L.J. & Brecht, M. Whisker movements evoked by stimulation of single motor neurons in the facial nucleus of the rat. *J. Neurophysiol.* **99**, 2821–2832 (2008).
27. Hall, R.D. & Lindholm, E.P. Organization of motor and somatosensory neocortex in albino rat. *Brain Res.* **66**, 23–38 (1974).
28. Sievert, C.F. & Neafsey, E.J. A chronic unit study of the sensory properties of neurons in the forelimb areas of rat sensorimotor cortex. *Brain Res.* **381**, 15–23 (1986).
29. Zhang, F. *et al.* Red-shifted optogenetic excitation: a tool for fast neural control derived from Volvox carteri. *Nat. Neurosci.* **11**, 631–633 (2008).
30. Graziano, M.S.A., Cooke, D.F., Taylor, C.S.R. & Moore, T. Distribution of hand location in monkeys during spontaneous behavior. *Exp. Brain Res.* **155**, 30–36 (2004).

nature | methods

Automated light-based mapping of motor cortex by photoactivation of channelrhodopsin-2 transgenic mice

Oliver G S Ayling, Thomas C Harrison, Jamie D Boyd, Alexander Goroshkov & Timothy H Murphy
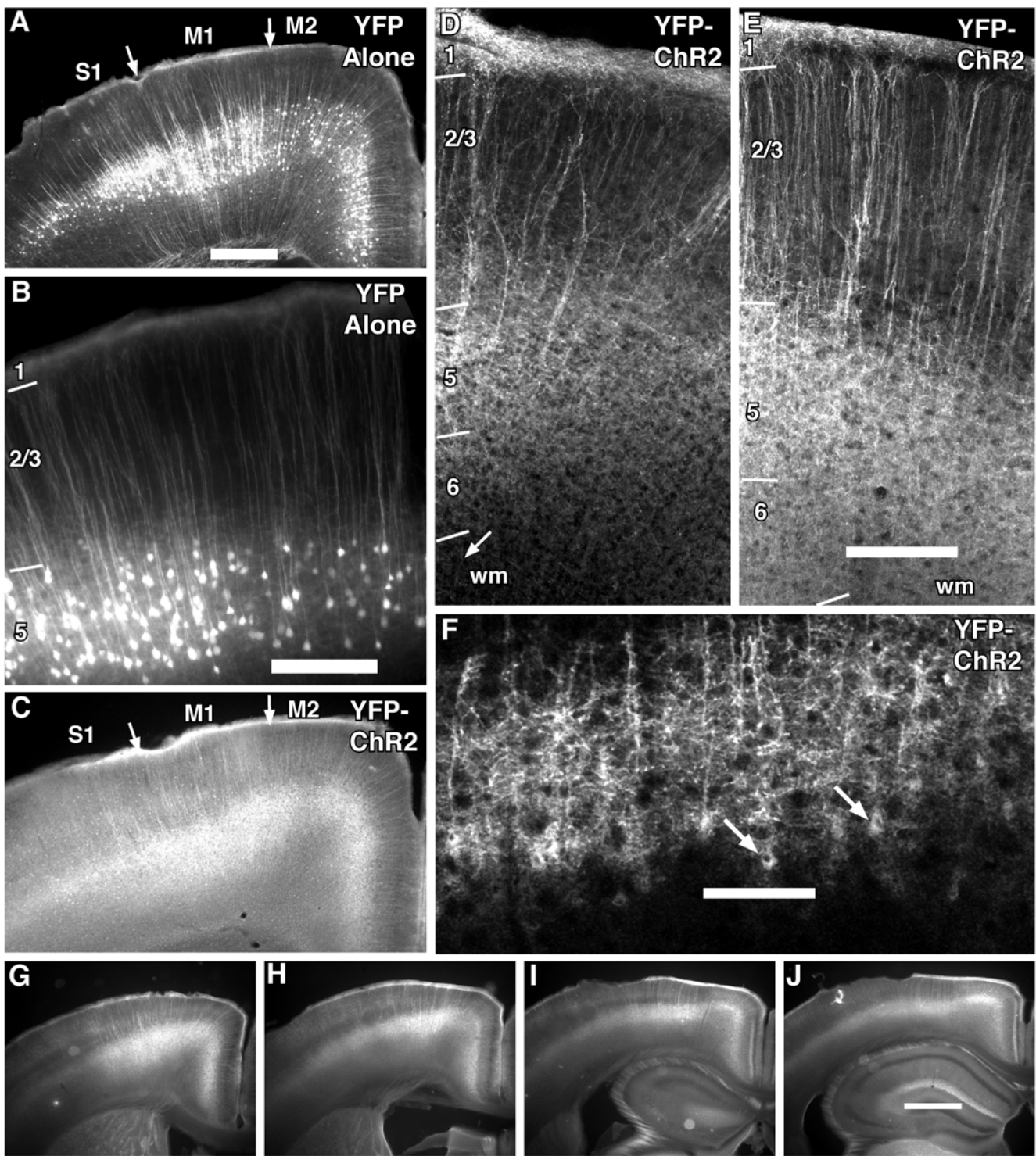
Supplementary figures and text:

Supplementary Figure 1	ChR2-negative animals show no response to photostimulation.
Supplementary Figure 2	ChR2 is expressed throughout the sensorimotor cortex in layer 5 cells.
Supplementary Figure 3	Response latency is inversely related to EMG amplitude.
Supplementary Figure 4	Glutamate receptor antagonist effect on light-evoked EMG and EEG activity.
Supplementary Figure 5	Estimates of CHR2 and ICMS electrode based cortical activation spread using IOS imaging.
Supplementary Figure 6	Focal and repeated photostimulation of motor cortex does not lead to degradation of motor map.
Supplementary Figure 7	Motor maps can be evoked weeks apart within the same animals.
Supplementary Figure 8	Stimulation-evoked movements detected by EMG and laser motion sensor.
Supplementary Table 1	Coordinates of the center point of cortical motor representations relative to bregma, as defined by two-dimensional Gaussian fitting.
Supplementary Table 2	Overlap of sensory and motor representations for forelimb and hindlimb ($n = 3$ mice).
Supplementary Methods	

**Supplementary Figure 1 ChR2-negative animals show no response to photostimulation.**
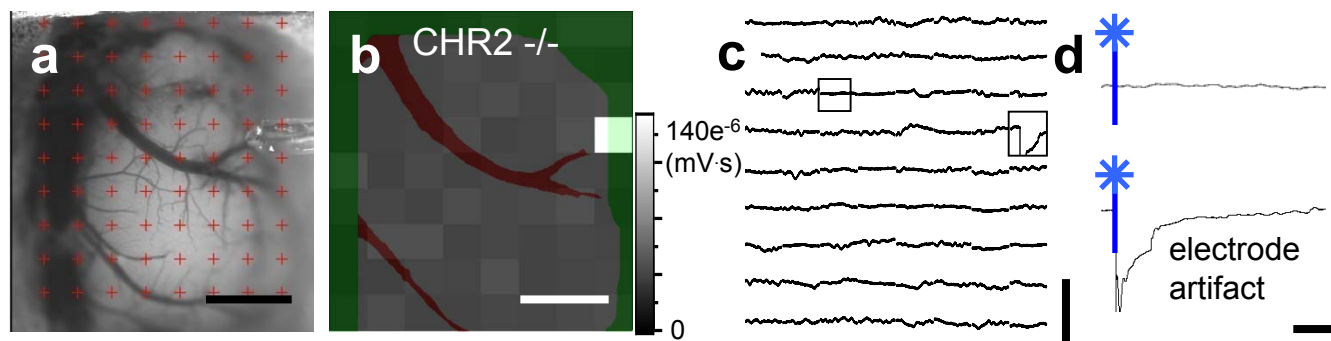
(**a**) Stimulation was delivered to an array of points (red crosses), and cortical activity was recorded by an EEG electrode (at right). (**b**) Each pixel represents the response evoked when the laser stimulated that cortical location, with lighter colors signifying a larger response. Scale bars in **a** and **b** 1 mm. (**c**) Raw EEG traces. Scale bars 3 mV, 200 ms. (**d**) selected traces enlarged from **c.** Note the large stimulation artifact produced when the laser strikes the recording electrode (bottom trace), which has amplitude and time kinetics dissimilar to genuine EEG responses. Scale bars 1 mV, 200 ms.

Supplementary Figure 2 ChR2 is expressed throughout the sensory-motor cortex in layer 5 cells.

Supplementary Figure 2 ChR2 is expressed throughout the sensory-motor cortex in layer 5 cells. Expression of YFP (**a**,**b**) and ChR2-YFP fusion protein (**c-f**) in fixed coronal sections of mouse cortex. Expression was under control of the *Thy1* promoter in both cases. (**a**) Low magnification wide-field fluorescence micrograph of a YFP-H mouse cortex. Medial is to the right and dorsal is to the top. Borders between primary motor cortex (m1), secondary motor cortex (m2), and primary somatosensory cortex (s1) are marked with arrows. Scale bar equals 500 μm, and also applies to **c**. (**b**) Higher magnification view of the border between m1 and m2. Apical dendrites of YFP-expressing neurons in layer 5 can be seen ascending to layer 1. Scale bar 250 μm. (**c**) Low power wide-field fluorescence micrograph from a mouse expressing the ChR2-YFP fusion protein. The areal and laminar expression pattern is similar to that shown in **a** for YFP expression in YFP-H line mice. (**d**,**e**) Maximum intensity projections over 20 μm from coronal slices of 2 mice expressing ChR2-YFP. Apical dendrites of layer 5 pyramidal neurons expressing ChR2-YFP extend into layer 1. No pyramidal neurons expressing YFP-ChR2 are seen in layer 2/3. Arrow in (**d**) shows an axon entering the white matter (wm). Scale bar in **e** equals 200 μm and applies to **f**. (**f**) Higher magnification maximum intensity projection of 3 μm through layer 5 from the same coronal slice illustrated in **d**. Examples of individual neurons expressing ChR2-YFP are indicated with arrows. Scale bar 100 μm. (**g-j**) Coronal sections (100 μm thick), anterior to posterior, of mice expressing ChR2-YFP, scale bar 1mm.

Supplementary Figure 3. Response latency is inversely related to EMG amplitude.
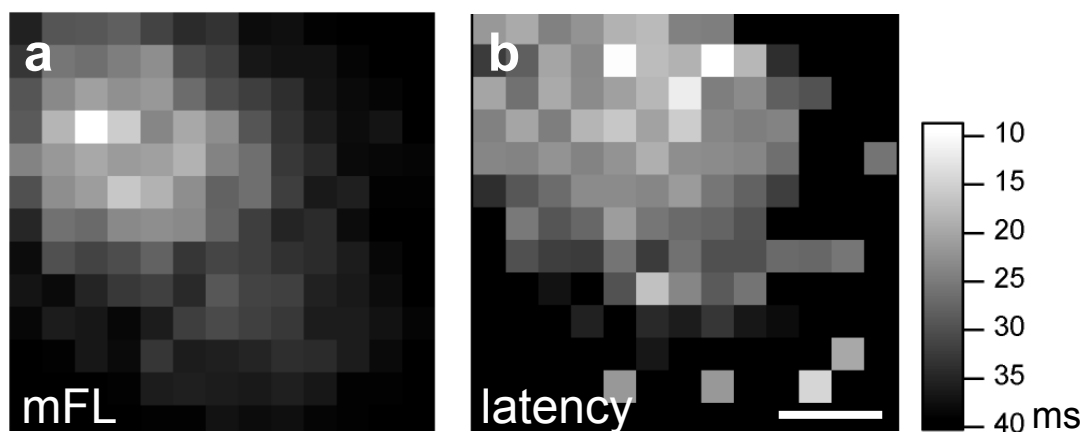
(**a**) High resolution forelimb motor map. White pixels are maximum EMG response, black is no response. Scale bar 1 mm. (**b**) Corresponding EMG latency map. Pixel values represent latency of EMG response from stimulus onset. Black pixels represent latencies greater than 40 ms or the absence of any response, white pixels represent latencies of less than 10 ms. Scale bar 1 mm.

Supplementary Figure 4. Cortical application of glutamate receptor antagonists have little initial effect on light-evoked EMG and EEG activity.
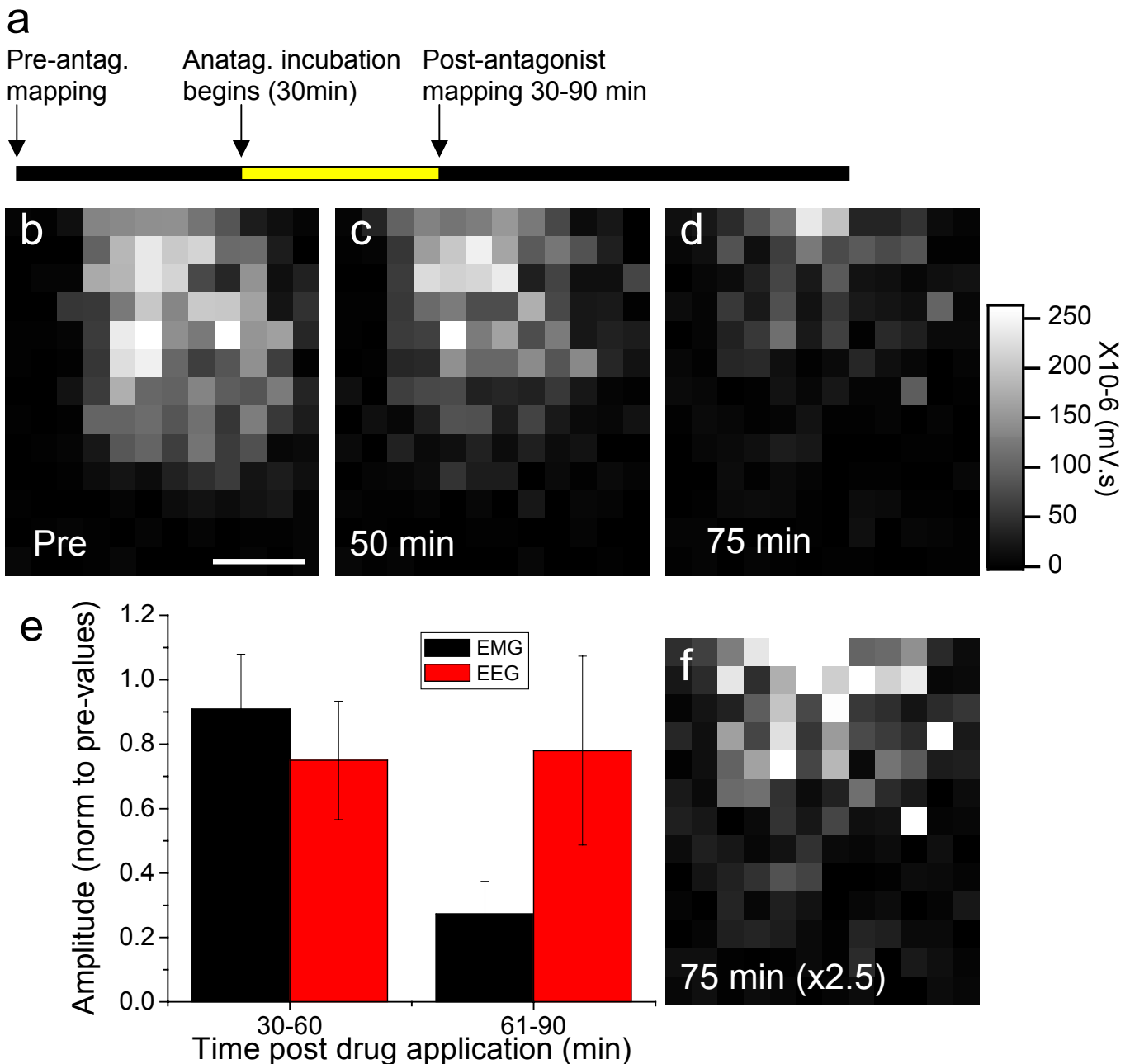

(**a**) Experimental timeline for antagonist experiments (MK-801 0.3 mM and CNQX 4.5 mM, applied directly to the intact cortical surface, dura intact). (**b**) Forelimb motor map before antagonist application. Scale bar, 1 mm. (**c**) Forelimb motor map 50 min after initial antagonist application. (**d**) Forelimb motor map 75 min after initial antagonist application. Motor map amplitude, indicated by the gray scale with scale bar expressed in mV·s on a linear scale. (**e**) EMG (black bars) and EEG (red bars) amplitudes normalized to pre-antagonist values (error bars SEM, n = 4 animals). Group data indicates that cortical EEG responses and light-evoked muscle potentials are relatively resistant to blockade of excitatory transmission in the cortex consistent with EMG maps reflecting direct activation of cortical spinal neurons and not indirect intracortical circuits. (**f**) Motor map in **d** with scale increased 2.5 times to highlight area of map rather than EMG amplitude.

Supplementary Figure 5. Estimates of CHR2 and ICMS electrode based cortical activation spread using IOS imaging.
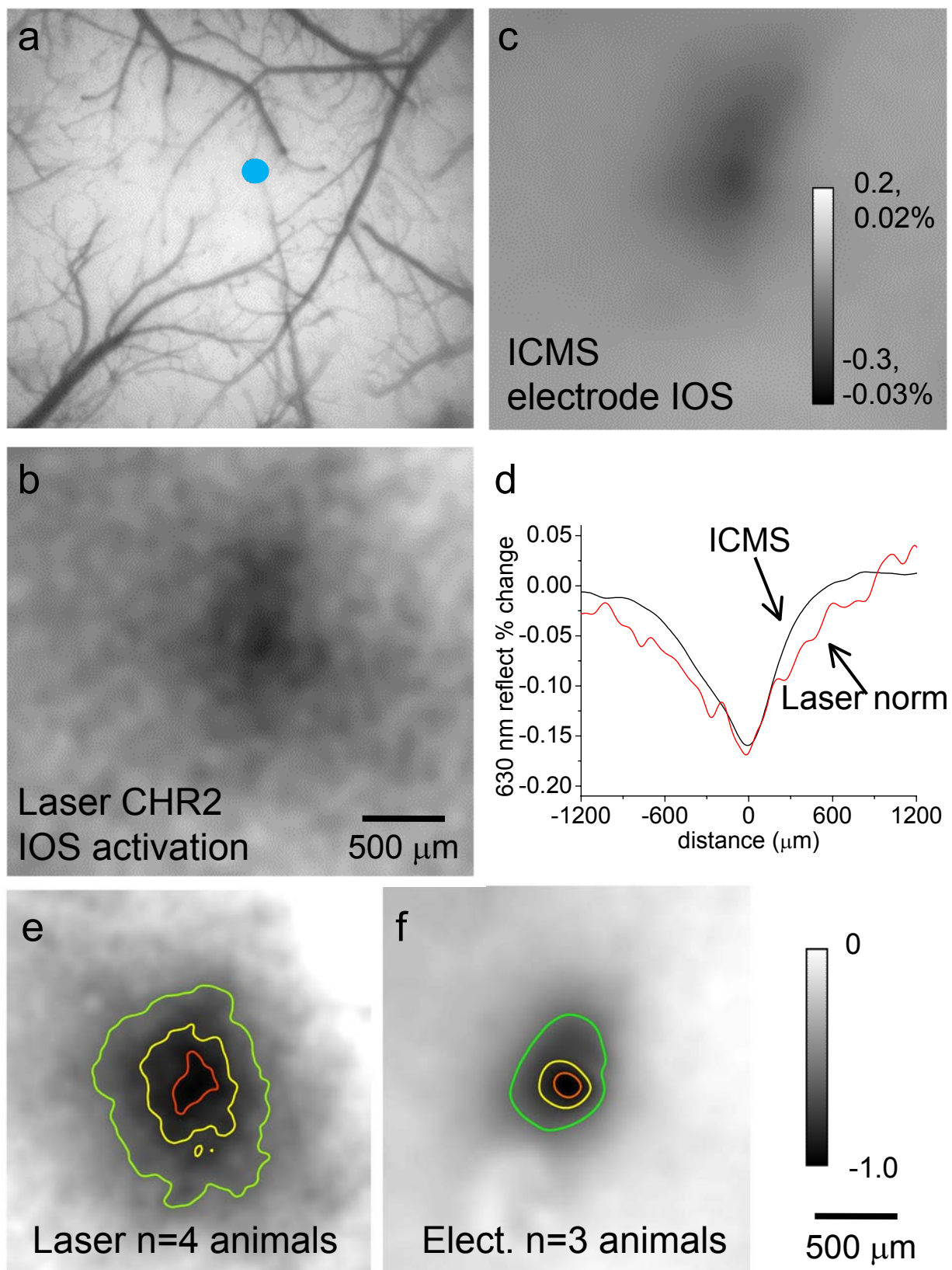
Supplementary Figure 5. Estimates of CHR2 and ICMS electrode based cortical activation spread using IOS imaging. (**a**) Image of brain surface with the location of blue laser light stimulation marked by a blue dot. A 100 ms train of 10, 5 ms laser pulses given at 100 Hz was used for optical stimulation. Intracortical microstimulation was performed in approximately the same area using a glass-stimulating electrode (see Supplementary Methods).
(**b**) Image showing change in reflected light signal 200 ms after the onset of a train of blue light pulses. A small reduction in reflected light is observed consistent with local brain activation. The scale for panel B is between -0.03 to +0.02 %; data is the average of 140 trials.
(**c**) Change in reflected light signal in response to ICMS train stimulation, the average of 60 trials is shown. (**d**) Plot of change in IOS reflectance measured using a horizontal rectangle 180 μm in height placed across the centre of activation for both channelrhodopsin activation and ICMS. The data plotted is from panels **b** and **c**. No light activated changes in brain reflectance were observed in 2 wild type animals examined, or in animals killed by anesthetic overdose.
(**e**) Average laser light-induced IOS response from normalized data (each animal scaled from -1.0 to 0) from n=4 animals using the parameters described above. Contour lines indicate 50, 75, and 90 % of the peak response in this panel and **f**.
(**f**) Average (ICMS) stimulating electrode induced IOS response from normalized data (each animal scaled from -1.0 to 0) from $n = 3$ animals using the parameters described above.

Supplementary Figure 6 Focal and repeated photostimulation of motor cortex does not lead to degradation of motor map.
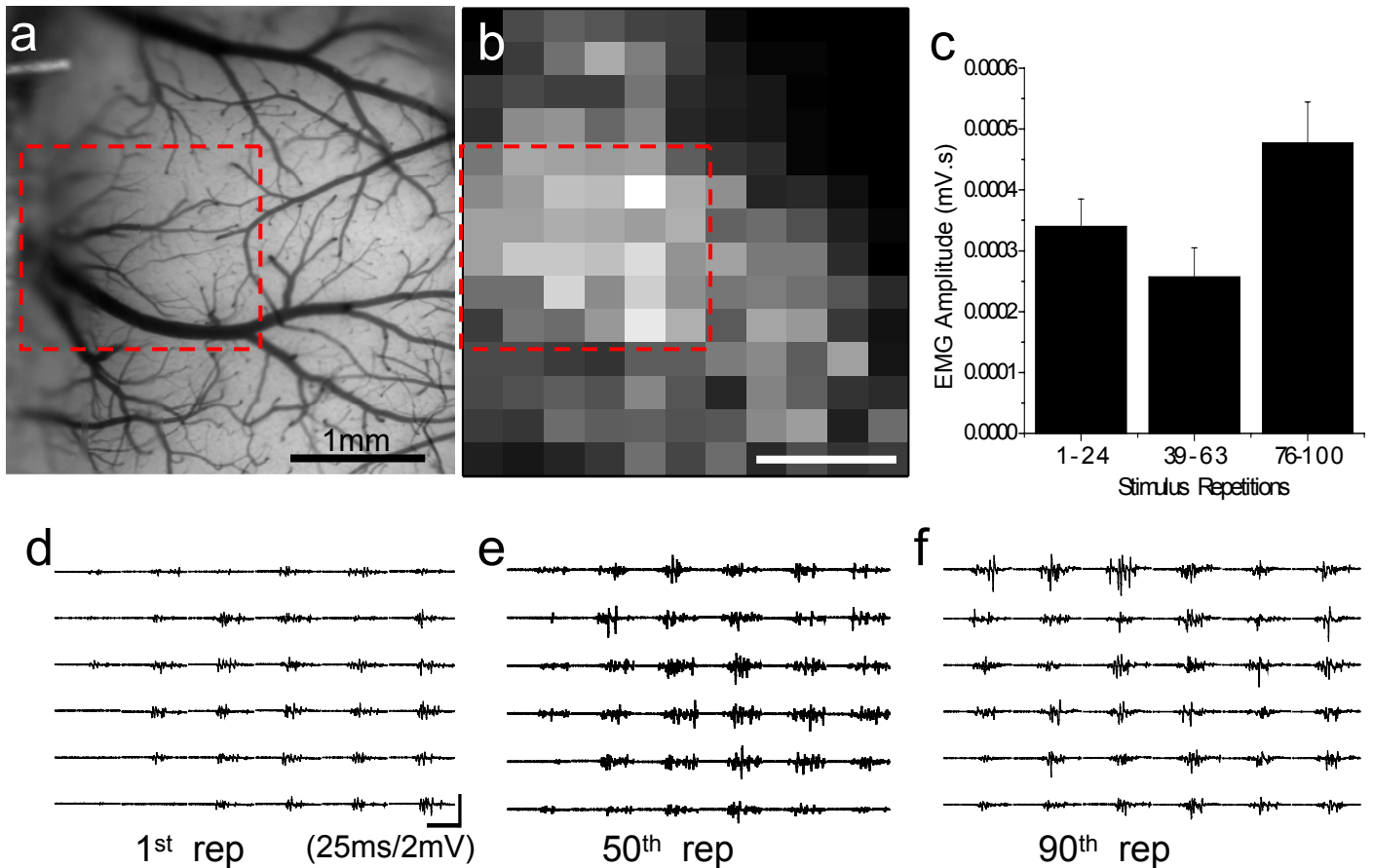
(a) Image of cortex with region of focal and repeated stimulation displayed in red box. 103 repetitions of a 6×6 pattern of photostimulation (300 µm spacing between points) was delivered to the same region of cortex prior to motor mapping (up to 294 mWmm^{-1} and 50 ms). (b) Forelimb motor map created after focal and repeated photostimulation. There is a robust response in area corresponding to the position of focal stimulation after 100 repetitions (red box). Scale bars, 1 mm. (c) Plot of EMG amplitude over multiple repetitions of photostimulation. EMG amplitudes are taken as the average of multiple repetitions from the area corresponding to the red box in **a** and **b** (error bars are SEM). (d-f) Raw EMG traces corresponding to red box in **a** and **b** taken from the 1st, 50th, and 90th repetition of focal photostimulation. Scale bar 25 ms, 2 mV.

Supplementary Figure 7. Motor maps can be evoked weeks apart within the same animals.

15 post-surgery days

25 post-surgery days

41 post-surgery days

48 post-surgery days
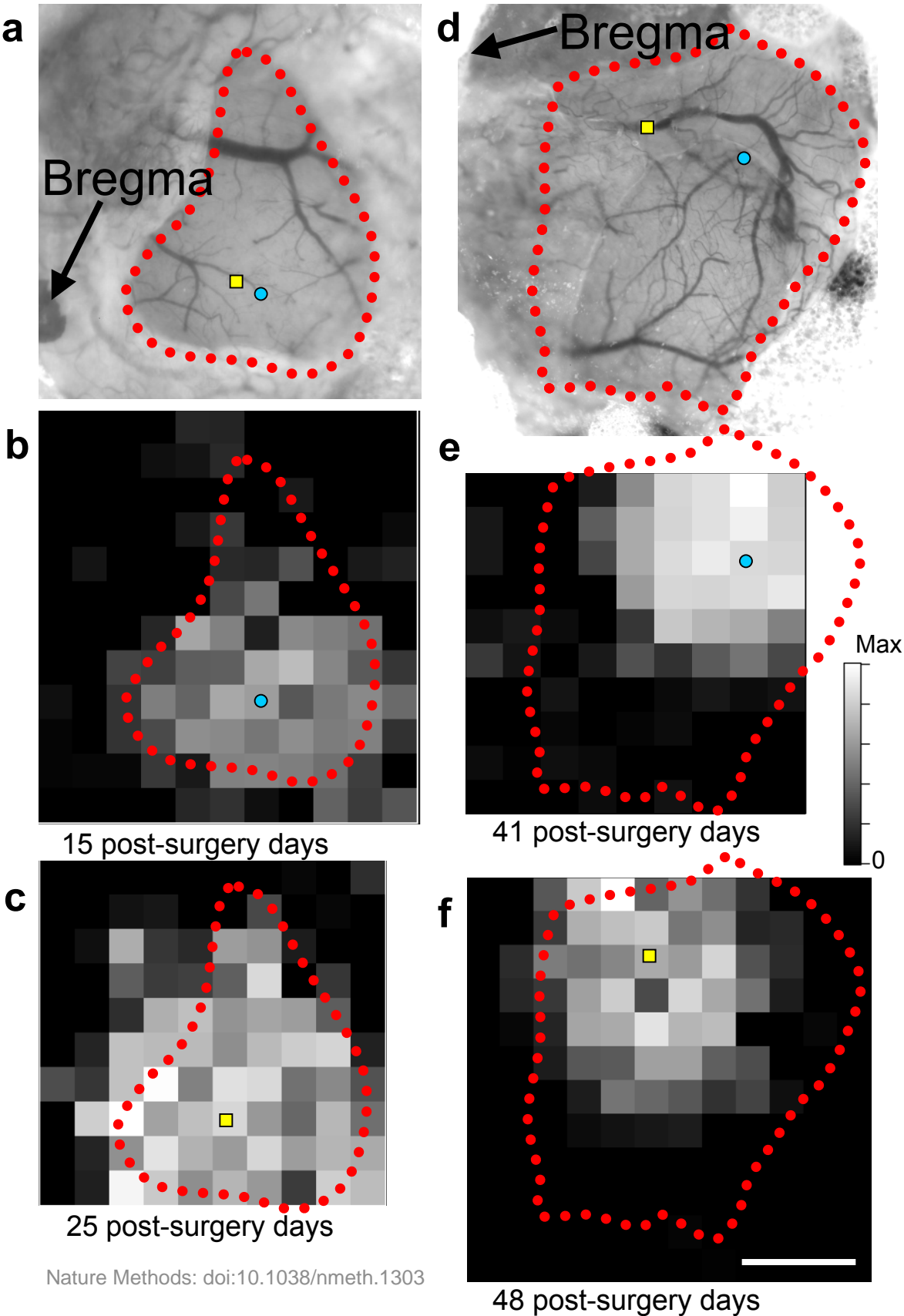
Supplementary Figure 7. Motor maps can be evoked weeks apart within the same animals. Preliminary maps of forelimb movements evoked by ChR2 activation within sensory-motor cortex from two separate animals implanted with chronic cranial windows are shown (measurements made with a laser-based motion sensor). The animal in (**a**) has been mapped two times (**b**,**c**), with one week between mapping sessions. The animal shown in panel (**d**) has been mapped three times, the second (**e**) and third (**f**) maps are shown here. The map centers (defined by 2-D Gaussian fit) are marked on each map and at the corresponding cortical location (in the top panel). The boundaries of the cranial windows are outlined in red. For all maps, black pixels represent cortical locations from which no movements were evoked, and white pixels represent the location of maximal response. Maps **b** and **c** are on the same scale, with black representing no evoked movement and white representing a limb displacement of 2.2 mm. Map **e** is similarly scaled from 0-4.6 mm, and **f** is scaled from 0-0.43 mm. Scale bar 1mm. Note that limb displacement is strongly dependent on anesthetic state and is highly variable.

Supplementary Figure 8. Stimulation-evoked movements detected by EMG and laser motion sensor.
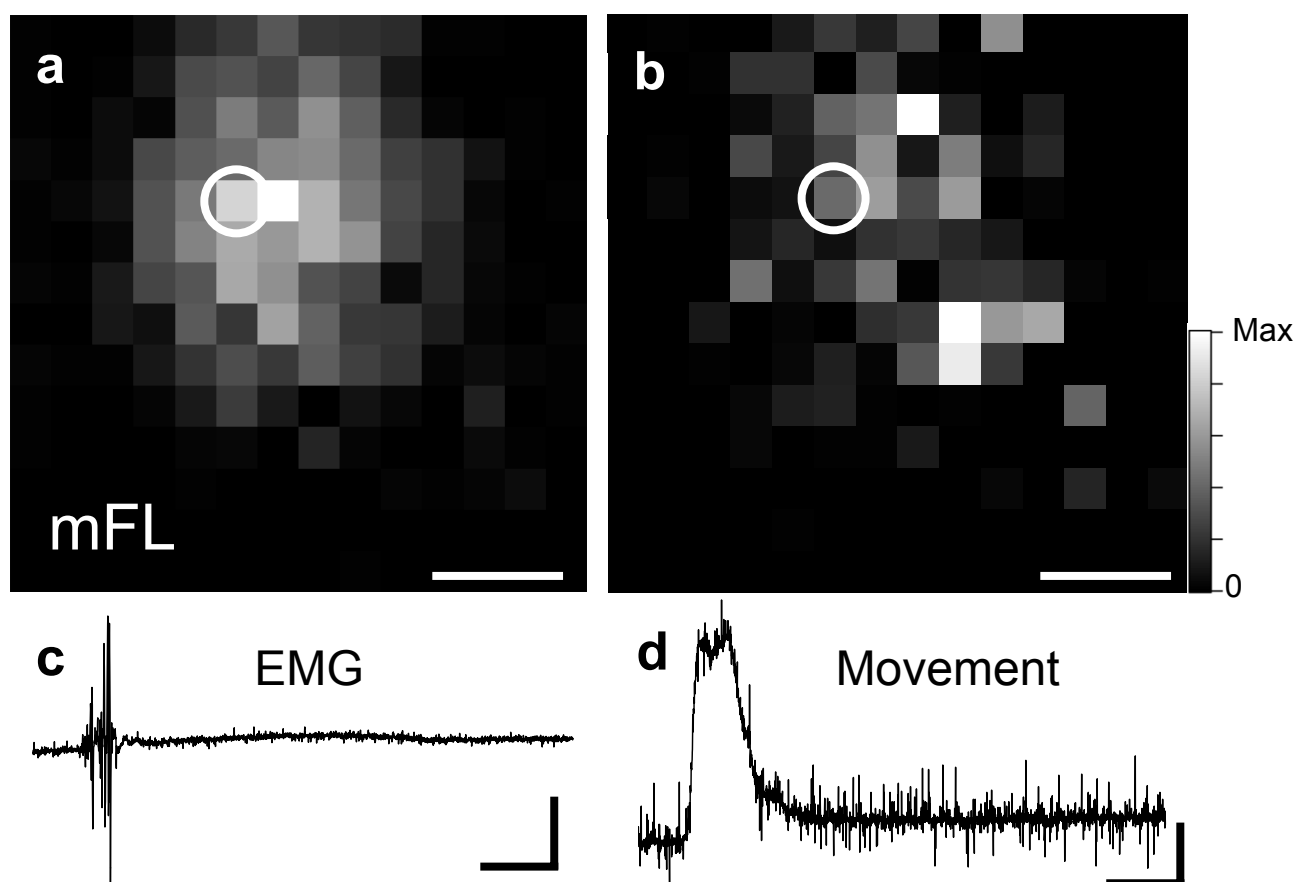
(**a**) EMG-based motor map of the extensor carpi radialis muscle. Pixel values signify EMG amplitude, with white corresponding to peak response and black to the absence of any response. (**b**) Forelimb movement map from the same animal obtained using a laser motion sensor. Pixel values correspond to the displacement of the forelimb, with values ranging from 15 mm (white pixels) to no movement. Scale bars 1 mm. (**c**) EMG trace corresponding to pixel circled in **a**. Scale bars 100 mV, 100 ms. (**d**) Laser motion sensor trace corresponding to pixel circled in **b**. Scale bar 0.5 mm, 100 ms.

Supplementary Table 1. Coordinates of the center point of cortical motor representations relative to bregma, as defined by two-dimensional Gaussian fitting. n=8 animals, with 3-6 maps per animal. Note, both HL and FL muscles were not always assayed within the same animals and inter-animal variability can account for some variability in map centers.

Muscle	Lateral from Bregma (mm)	Posterior from Bregma (mm)
Extensor carpi radialis brevis (FL extensor)	1.84+/- 0.37	0.42 +/- 0.97
Triceps brachii (FL extensor)	1.96 +/-0.29	0.15 +/- 0.66
Biceps femoris (HL flexor)	1.47 +/- 0.32	0.55 +/- 1.04
Vastus lateralis (HL extensor)	1.60 +/- 0.25	-0.33 +/- 0.97

Supplementary Table 2. Overlapping sensory and motor representations of forelimb and hindlimb (n=3 mice).

Muscle	% Motor map in sensory territory.	% Motor map in FL sensory territory	% Motor map in HL sensory territory
Extensor carpi radialis brevis (FL extensor)	51 ±15	24 ±8	27 ±8
Triceps brachii (FL extensor)	51 ±12	22 ±10	29 ±4
Biceps femoris (HL flexor)	55 ±14	0 ±0	55 ±14
Vastus lateralis (HL extensor)	50 ±12	3 ±5	47 ±11

Results of one-way ANOVA $F_{(7, 16)}$ = 14.668, $p < 0.0001$, Bonferroni post-hoc test

Comparison	Mean Difference	P value
Biceps femoris FL sensory overlap vs. Biceps femoris HL sensory overlap	-55.39	P<0.001
Biceps femoris FL sensory overlap vs. Vastus lateralis HL sensory overlap	-46.70	P<0.001
Vastus lateralis FL sensory overlap vs. Biceps femoris HL sensory overlap	-52.50	P<0.001
Vastus lateralis FL sensory overlap vs. Vastus lateralis HL sensory overlap	-43.81	P<0.001

Supplementary Methods

Animals and surgery

Adult mice aged 2-3 months and weighing 25-30 g were used for these experiments, and were maintained on a 12:12 hour light:dark schedule. Anesthesia was induced with isoflurane (1.5 % in air) and body temperature was maintained at 37° C ± 0.5° C using a feedback-regulated heating pad. A craniectomy was made over the right sensory-motor cortex while the anesthetized mouse was supported by ear and tooth bars. The skull was then fastened to a stainless steel plate[1] with cyanoacrylate glue and dental cement, and the plate attached to 25.4 mm posts mounted on an aluminum plate that could be bolted to a stage. The exposed brain was covered with 1-1.5 % agarose (Type 3-A Sigma; A9793) dissolved in a HEPES buffered (pH 7.3) physiological salt solution (in mM): 135 NaCl, 5.4 KCl, 1 $MgCl_2$, 1.8 $CaCl_2$, and 5 HEPES, and sealed with a custom cut glass coverslip. Isoflurane anesthesia was maintained during IOS imaging of somatosensory representations, but was replaced by ketamine/xylazine prior to LBM. Consistent with previous work[2, 3], we found it easier to elicit an evoked response in ketamine/xylazine anesthetized animals. Ketamine/xylazine was administered in doses of 0.02 mL (20 mg mL^{-1} ketamine, 2 $mgmL^{-1}$ xylazine) approximately every 30 minutes or as necessary to maintain a constant level of anesthesia.

Optical imaging and photoactivation

To perform IOS imaging and to create maps of the surface vasculature a Dalsa 1M60 camera was used (Waterloo Ont. Canada). The frame grabber for the camera was

an E1DB from EPIX (Buffalo Grove IL USA) and was running EPIX XCAP version 2.2 software. The camera was mounted on a vertical milling machine (Sherline Tool #5430, Miami FL USA), and images were taken through a macroscope composed of front-to-front video lenses coupled with a 52 mm threaded adaptor ring (BH Photo, New York NY USA). The top lens (closer to the camera) was a 135 mm F2.8 Nikor and the lower lens was a 50 mm F1.4 Nikor lens. To direct the 473nm photoactivation laser (CrystaLaser BCL-473-050, Reno NV USA) a hole was cut in the side of the Dalsa 1M60 camera F-mount adaptor and a dichroic mirror was installed between the CCD camera and the first video lens. The dichroic mirror was an Olympus DM500 (500nm cut-off). To direct the blue laser light an optical cage was constructed using Thorlabs 5 mm rods and microbench parts similar to that previously reported by us for photoactivation of rose bengal[4].

There are several possible methods for photoactivation of ChR2 transgenic mice[5]. Fiber optic systems are the best option for targeting subcortical structures, but are not ideal for stimulating the cortical surface because of light divergence[6]. Divergence becomes a considerable problem in mapping, where curvature of the brain results in a variable distance between the light source and cortical surface. By using lens based beam-conditioning optics we were able to generate a relatively collimated beam that could be varied in size from 100 to 220 μm in diameter by changing lens focal lengths and/or lens positions. Within the optical cage, a 25.4 mm plano convex 50 mm focal length lens (LA1131, Thor Labs, Newton NJ USA) could be moved relative to the first video lens (typically placed 145 mm from the first video lens) to alter the laser spot size on the brain surface. The beam XY position within the video image field could be

adjusted by moving both the plano convex lens within its mount using a Thorlabs XY translator lens mount (HPT1) as well as a right angle silver mirror mounted on a XY adjustable holder (Linos 065087, Goettingen, Germany) within a 30 mm Linos cube (061081). A final level of adjustment was achieved using a Linos XY adjustable holder (065087).

The XY stage used to move the animal relative to the laser was driven by XY LS50 high-velocity motors and controlled by an MS2000 2-axis stage controller (Applied Scientific Instrumentation, Eugene OR USA). All maps were created based on a random sequence of movements to a series of positions outlined in a grid of stimulus locations superimposed over a map of the brain (see Software section below for details). We chose a stage scanning system since it was capable of repeated optical stimulation at intervals of < 1 s and ensured accurate XY positioning. An advantage of a mechanical scanning system is that all movements are based on absolute distance with respect to the excitation laser, and therefore it is inconceivable that photoactivation power or position would be subject to errors due to lens aberration that may occur near the edges of an image field. Although it would be possible to reduce the time between stimulation points by using a galvanometer and mirror based beam steering system, shorter (< 1 s) interstimulus intervals may lead to unexpected interactions between stimulus pulses. For both EEG and EMG maps, stimulus parameters (especially duration) were increased gradually until deflections in the recorded traces became apparent upon visual inspection. Once this threshold was reached, we would increase the stimulus duration by an additional 50 % to ensure adequate stimulation.

3

Testing for the effect of photodamage on motor maps

To test for photodamage, we compared processed forelimb EMG responses from two animals evoked by stimulation within a region of interest (a square of 36 pixels, each pixel 300 μm^2). We compared EMG responses from stimulus parameters for trials at the beginning and the end of an experiment. In one animal, there was no significant difference in evoked EMG amplitude after 143 intervening stimulus trials ($P = 0.1220$, paired t-test). The other animal showed an increase in EMG amplitude after 103 trials of stimulation ($P = 0.0004$, paired t-test), which is explainable by a decrease in anesthetic depth or stimulation-induced plasticity (**Supplementary Fig. 6**)

The laser powers used (40-600 mWmm^{-2}, 1-35 ms) were within the limits of the maximum permissible exposure to the human cornea[7] (for 1 Wmm^{-2}, the maximum permissible exposure time specified by IEC 60825 standards is 1ms for lasers with wavelengths 400-700 nm).

IOS

Prior to each motor mapping session, we conducted IOS imaging to define the locations of the somatosensory forelimb and hindlimb representations. Following a protocol described previously[8], we used piezoceramic bending actuators (Piezo Systems Q220-AY-203YB, Cambridge MA USA) to deliver 1 s trains of 100 Hz vibrations to the forelimb and hindlimb alternately. 15 baseline images were compared to 15 images captured over a 1.5 s period following stimulation, and a custom-written ImageJ (NIH, Bethesda MD USA) plugin was used to calculate the percentage change in reflectance of 635 nm light. A 50 % threshold was then applied and the resulting maps color-coded.

4

ICMS

ICMS was performed using a glass pipette (2-3 MΩ, made on a Narashige P_83 vertical electrode puller) containing a 0.25 mm bare silver wire and filled with 3 M sodium chloride, with fast green (Sigma) added in order to facilitate visualization under the microscope. Five to ten 125 ms trains of stimulation, each with five 240 μs stimuli at maximum intensities of 200 μA, were delivered at a frequency of 40 Hz to a depth of 400-500 μm to target layer 5 motor neurons. Impalement sites were guided by somatosensory IOS maps, and spacing between sites was approximately 500 μm. EMG latencies for ICMS and LBM were calculated by measuring from stimulus onset to the point where a pre-defined threshold was exceeded (three times the standard deviation of the baseline noise).

Motor output recordings

Hindlimb EMGs were recorded from the biceps femoris and the vastus lateralis muscles using electrodes similar to those described by others[9]. These were constructed by twisting together a pair of 0.125 mm teflon coated silver wires and stripping the insulation from two non-overlapping contacts. The twisted bipolar electrodes were then inserted into the muscle using a 22.5-gauge needle. The forelimb EMG recordings were made from the triceps brachii and the extensor carpi radialis brevis muscles using single 0.125 mm teflon wires bared 2 mm from the end and inserted with a 26-gauge needle. The insulated tips of the wires were then bent over to secure them in place. A common ground for the two forelimb electrodes was inserted into a small incision in the footpad.

The larger twisted bipolar electrodes were used exclusively in the hindlimb because of the small size of the forelimb muscles. Forelimb movements were also quantified using a laser motion sensor (LK-2000, Keyence, Osaka Japan).

EEG

To examine stimulation-evoked EEG responses at the cortical surface, we used a razor blade to bare ~1 mm from the tip of 125 μm diameter silver wires. The electrodes were inserted into the agarose near each of the four corners of the craniectomy. We then mapped the entire surface of the exposed cortex, performing 3-5 repetitions per map. The averaged maps recorded by each electrode were then normalized to each other and a mean map incorporating the information from all electrodes was created. The duration of individual EEG depolarizations was measured from stimulus onset to the time point where the trace returned to 85 % of the pre-stimulation baseline. EEGs and EMGs were sampled at 5 kHz. An unpaired t-test was used to compare stimulus duration vs. EEG depolarization duration.

Effects of glutamate receptor antagonists on EMG maps.

Although light activation may be targeted to a selected region, adjacent areas of cortex could be activated through intra-cortical synaptic interactions. We have addressed this possibility by applying AMPA/NMDA glutamate receptor antagonists to the surface of the cortex at high concentrations that we have previously been shown to completely block sensory stimulation induced intrinsic optical signal maps (supplementary Fig. 4). These maneuvers would be expected to block intracortical synaptic transmission and

potentially the spread of excitation. Despite using these antagonists, we found only modest change in the size area or amplitude of the light activated maps within the first 30-60 min. These experiments were performed as follows. After obtaining a set of baseline maps as described above, we applied CNQX (4.5 mM) and MK801 (300 μM, both in physiological saline solution) to the open craniectomy (with dura intact) and allowed the drugs to incubate for 30 minutes. Motor mapping resumed following this period and lasted for up to two hours after the incubation period. The drugs were reapplied (at the same concentrations) to the cortical surface at intervals of approximately 30 min. To compare EMG amplitudes before and after application of the drugs, we calculated mean amplitudes for a region of 12 pixels (3×4) at the center of the motor map (as defined by a two-dimensional Gaussian fit). Paired t-tests were used to compare EMG and EEG amplitude at time points after drug application (30-60, 61-90 min) to pre-drug EMG and EEG amplitudes. Glutamate antagonists failed to have a significant effect on motor map amplitude ($P = 0.1393$, $n = 14$ maps from four mice, paired t-test), or the cortical EEG ($P = 0.0595$, $n = 10$, paired t-test) elicited by light stimulation within 30-60 min of application in 5 of 6 animals examined (**Supplementary Fig. 4**). At later time points (90 min) map amplitude was depressed ($P < 0.0001$, $n = 12$ maps from four mice, paired t-test) (possible due to more distant drug action), but map boundaries were in part retained. A total of 5 animals were studied for comparison of EEG and EMG sensitivity to antagonists; one animal was not included since the EMG amplitude decreased by over 80 % within the first 30 min of antagonist application and the EEG was of poor quality compared to the results observed in the other 4 animals.

These observations suggest that light-based motor maps are not necessarily dependent on intracortical synaptic activity. At longer time points (90 min after MK801 and CNQX addition) we did observe an 80 % depression of map amplitude. We are currently are exploring why the drugs had a delayed effect on amplitude, but presumably this reflects a more distant site of action, perhaps near the layer 5 somata or within the striatum or spinal cord. Nonetheless, despite pharmacological diminution of the maps by a factor of 3 in the amplitude, their general boundaries still apparent (**Supplementary Fig. 4**). This result is consistent with light-based mapping directly activating layer 5 output neurons leading to muscle potentials rather than a model where light-based pulses activate intracortical synaptic transmission, which does not necessarily reflect direct connections from motor cortex.

Characterization of photoactivation area.

We used IOS imaging using 630 nm illumination as described above to assess the spread of laser excitation following photostimulation. We compared 15 baseline images to 2 images collected 200-400 ms after photostimulation (100ms burst of 5 ms pulses delivered at 100 Hz with laser power between 156 and 469 mWmm^{-2}. We also used an intracortical microelectrode (see ICMS section above) to deliver a 100 ms 100 Hz train of 200 µA of stimulation pulses using the parameters employed for ICMS. To obtain reliable IOS activation using the ICMS electrode we needed to increase the pulse duration to 5 ms. In analysis of 2 animals we found that varying the ICMS pulse duration from 0.5-5 ms did not strongly affect the width of the IOS activation ($r^2 = 0.325$). The photoactivation profile was estimated from average images of changes in light reflectance

and measuring the full width at half maximal amplitude of the response as well as a contour plot analysis of averaged group data (**Supplementary Fig. 5**).

Software

Custom software in Igor Pro (Wavemetrics) running on a standard PC controlled the scanning stage using serial commands, while a National Instruments board (PCI-6036E) triggered the 473 nm laser with a TTL pulse and acquired analog outputs (5 kHz) from EEG, EMG, and the laser motion sensor. The software package includes a graphical user interface that allows the experimenter to modify all parameters of interest (e.g. stimulus duration, number of repetitions, inter-stimulus delay, channels recorded, sampling rate etc.). Within each repetition, stimuli were always delivered in a randomized fashion. Randomization was achieved by sorting the list of desired stimulation points by a list of random numbers generated by the Igor Pro random number function. At the beginning of each experiment, the number and location of stimulation points were defined with reference to an image of the exposed brain.

EMG and pixel based motor map analysis

EMG records were sampled at 5kHz, and band-pass filtered (0.5-500 Hz), full-wave rectified, the mean of the pre-stimulation baseline subtracted, and integrated to give the array of values displayed in pixel-based maps. In order to quantify the size of motor maps and locate their centers, we fitted a two-dimensional Gaussian curve to the pixel-based maps. Motor and sensory map areas were estimated from contour lines of Gaussian fits at 50 % of peak value. The mean areas of the Gaussian-fit cortical representations of

the four muscles studied were then determined (n=9 animals), and a one-way ANOVA was performed ($P = 0.0006$) followed by the Tukey-Kramer multiple comparisons test. The baseline offset of each Gaussian fit (z0) was defined as the mean of the background noise. This value was obtained from trials in which stimulation was targeted over thick bone, where no response should be evoked. In approximately 5 % of cases, the maps were of relatively poor quality and could not be fit by the Gaussian function. Maps were excluded from further analysis if any of the following three empirically established criteria were not met: peak amplitude of map is more than five times greater than the standard deviation of the baseline noise; map width is at least 300 μm (typical size of one pixel) in the X and Y dimensions; and calculated map center must be within the area selected for photoactivation and imaging. Poor map quality could generally be attributed to imperfect craniectomies or anesthesia. The X and Y values of the map centers and widths were then averaged across several maps (3-6 per animal), and the means of these values were compared statistically. Before performing one-way ANOVA on the map area values of the different muscles, we tested the variation of the standard deviations and found that it was not significant ($P = 0.131$, Bartlett test). Because we did not record from all four muscles in some animals and because some maps were excluded, not all comparisons were made using the same number of animals. To generate maps based on laser motion sensor data, a two-sided Gaussian fit was applied to each trace and the peak displacement was plotted for each point of stimulation.

Histology

Brains were fixed for histology by transcardial perfusion with 4% paraformaldehyde and, coronal slices 100μm thick were sectioned by vibratome and examined under epifluorescence as described by Brown *et al.*[10]. Confocal microscopy image analysis was performed with 16 bit, 20 and 40x magnification at 1.6 and 3.2 μm pixel^{-1}.

LITERATURE CITED

1.   Kleinfeld, D. & Denk, W. Two-photon imaging of neocortical microcirculation. in *Imaging neurons: a laboratory manual* (ed. R. Yuste, F. Lanni & A. Konnerth) 23.21-23.15 (Cold Spring Harbor Laboratory Press, Cold Spring Harbor, NY, 2000).
2.   Hosp, J.A.*, et al.* Thin-film epidural microelectrode arrays for somatosensory and motor cortex mapping in rat. *J. Neurosci. Methods* **172**, 255-262 (2008).
3.   Ferezou, I.*, et al.* Spatiotemporal dynamics of cortical sensorimotor integration in behaving mice. *Neuron* **56**, 907-923 (2007).
4.   Sigler, A., Goroshkov, A. & Murphy, T.H. Hardware and methodology for targeting single brain arterioles for photothrombotic stroke on an upright microscope. *Journal of Neuroscience Methods* **170**, 35-44 (2008).
5.   Arenkiel, B.R.*, et al.* In vivo light-induced activation of neural circuitry in transgenic mice expressing channelrhodopsin-2. *Neuron* **54**, 205-218 (2007).
6.   Aravanis, A.M.*, et al.* An optical neural interface: in vivo control of rodent motor cortex with integrated fiberoptic and optogenetic technology. *J. Neural Eng.* **4**, S143-S156-S143-S156 (2007).
7.   Lund, D.J., Stuck, B.E. & Edsall, P. Retinal injury thresholds for blue wavelength lasers. *Health Physics* **90**, 477-484 (2006).
8.   Winship, I.R. & Murphy, T.H. In vivo calcium imaging reveals functional rewiring of single somatosensory neurons after stroke. *J. Neurosci.* **28**, 6592-6606 (2008).
9.   Pearson, K.G., Acharya, H. & Fouad, K. A new electrode configuration for recording electromyographic activity in behaving mice. *Journal of Neuroscience Methods* **148**, 36-42 (2005).
10.   Brown, C.E., Li, P., Boyd, J.D., Delaney, K.R. & Murphy, T.H. Extensive turnover of dendritic spines and vascular remodeling in cortical tissues recovering from stroke. *J. Neurosci.* **27**, 4101-4109 (2007).